



## **SIMULATION OF NONSTATIONARY GROUND MOTIONS USING WAVELETS**

**Jeremiah LEGRUE<sup>1</sup> and Charles MENUN<sup>2</sup>**

### **SUMMARY**

Investigations of damage caused by near-field ground motions have shown that structural response, especially in the nonlinear range, is sensitive to the amplitude and duration of acceleration and velocity pulses present in the input ground motion. This paper describes a procedure that utilizes the wavelet decomposition of a recorded accelerogram to simulate an ensemble of ground motions that have localized temporal features and variations in the frequency content that are similar to those present in the original record. Ensembles of simulated ground motions are generated using the proposed method for ten near-field accelerograms. It is found that the significant temporal features present in the target accelerograms are closely reproduced in the simulations, and the ensemble response spectra, on average, closely match the target response spectra over a wide range of frequencies. A nonlinear model of a nine-story building is analyzed using the wavelet-based ground motion ensembles and a second set of ensembles generated with the ARMA method. Structural response produced by the wavelet-based simulations shows closer agreement with the target accelerograms than the response produced by the ARMA simulations.

### **INTRODUCTION**

Numerous studies, including those made by Anderson [1], Hall [2], and MacRae [3], indicate that structures experience increased inelastic demands when subjected to near-field ground motions. For example, an extensive study of the Olive View Hospital, which was heavily damaged in the 1971 San Fernando earthquake, revealed that the primary cause of damage was a long-duration acceleration pulse that occurred approximately three seconds into the recording, not the large amplitude, short duration acceleration spike that occurred five seconds later (Bertero [4]). The importance of the acceleration pulse as an indicator of damage potential has been well documented (Anderson [1]).

Because the response of nonlinear structures can be sensitive to temporal variations in the intensity, frequency content and phasing of the seismic input, an important aspect of such analyses is the selection of the ground motions to be used. Ideally, one would like to use an ensemble of recorded ground motions that are representative of the seismic environment of the building site. However, due to the paucity of recorded ground motions in near-fault environments, such ensembles cannot always be assembled from

---

<sup>1</sup> Design Engineer, Hohbach-Lewin, Inc. Email: jlegrue@hohbach-lewin.com

<sup>2</sup> Assistant Professor, Stanford University. Email: menun@stanford.edu

historical records alone. Consequently, there is a need for simulated strong ground motions to augment the historical database.

This paper describes a wavelet-based ground motion simulation procedure. Wavelet analysis is well-suited to identifying and preserving nonstationarity because the wavelet basis consists of compact functions of varying lengths. Each wavelet function corresponds to a finite portion of the time domain and has a different bandwidth in the frequency domain. The multiscale nature of wavelet analysis facilitates the simultaneous evaluation of nonstationarity in the time and frequency domains. Wavelet analysis has been applied to engineering problems by several authors. Newland [5,6] used wavelets to analyze structural vibrations due to underground and surface traffic. Gurley and Kareem [7] examine a variety of applications for wavelet analysis including two general methods for simulating nonstationary processes. Given a target signal, evaluating its wavelet transform and multiplying each wavelet coefficient by a unit-variance Gaussian random variable can produce realizations that are similar to the target. If a target power spectrum is given, a different modulating function can be used for each wavelet frequency band following a procedure similar to Priestley's evolutionary spectrum [8]. The procedure proposed by Iyama [9] is similar to the latter method. A bilinear target spectrum is used for simplicity and the modulating functions, which are expressed as energy release rates, are cubic polynomials.

The objective of the proposed procedure is to use the wavelet decomposition of a recorded ground motion to generate simulations that have localized temporal features and variations in the frequency content that are similar to those present in the original record. Because the proposed procedure simulates ground motions in a numerical manner without consideration of the physics that caused the recorded accelerogram (e.g., the faulting mechanism, the propagation and attenuation of seismic waves from the fault to the building site, etc.), it is properly classified as a stochastic ground motion model. Stochastic ground motion simulation procedures that are currently available include spectral methods [e.g., 10,11], autoregressive moving average (ARMA) models [e.g., 12,13], and Fourier phase difference models [e.g., 14]. As mentioned above, the proposed wavelet-based procedure uses a recorded accelerogram as a basis for the simulated ground motions. Consequently, the implementation of the procedure is similar to that of ARMA and Fourier phase difference methods that use recorded "target" accelerograms to identify the parameters that define the ground motion model. The advantage of the wavelet-based procedure over these existing techniques stems from the fact that wavelets are compact and are therefore able to accurately preserve time-dependent features present in a recorded signal.

Application of the proposed procedure is demonstrated by analyzing a nonlinear model of a nine-story building with ensembles of wavelet-based and ARMA-generated ground motions. These analyses demonstrate that the structural response produced by the wavelet-based simulations is in closer agreement with that produced by the target accelerograms than the response produced by the ARMA simulations.

## WAVELETS

The wavelet transform of a signal  $f(x)$  consists of a set of functions (wavelets) that can be recombined to recover the original signal. The wavelets can be written in terms of the mother wavelet,  $\psi(x)$ , as

$$\psi_{j,k}(x) = 2^{j/2} \psi(2^j x - k) \quad (1)$$

where the scale,  $j$ , and translation,  $k$ , are elements of  $\mathcal{Z}$  the integers. The scale parameter determines the length of the wavelet function and the translation parameter determines where it is located on  $\mathfrak{R}$ , the real numbers. We use the term wavelet level to denote the subset of wavelets corresponding to a particular value of  $j$ . Wavelet functions are more compact at higher levels; i.e., a wavelet at level  $j$  spans a shorter domain than a wavelet at level  $j - 1$ . However, the set of wavelet functions at each level spans  $\mathfrak{R}$ . For any  $J \in \mathcal{Z}$ , the collection  $\{\varphi_{J,k}(x)\}_{k \in \mathcal{Z}} \cup \{\psi_{j,k}(x)\}_{j \geq J, k \in \mathcal{Z}}$  forms an orthogonal basis on  $\mathfrak{R}$  where  $\varphi_{J,k}(x)$  is defined

in terms of the scaling function,  $\varphi(x)$ , as

$$\varphi_{j,k}(x) = 2^{j/2} \varphi(2^j x - k), \quad (2)$$

where, again,  $j, k \in \mathbb{Z}$  (Walnut, [15]).

From the many wavelets that are available, the D20 wavelet was chosen for this study because it is compact and the D20 wavelet function is nearly band-limited. Figure 1 shows the D20 wavelet function at several different wavelet levels. Note that at higher levels, the domain over which the wavelet takes non-zero values decreases, but the shape of the function remains the same.

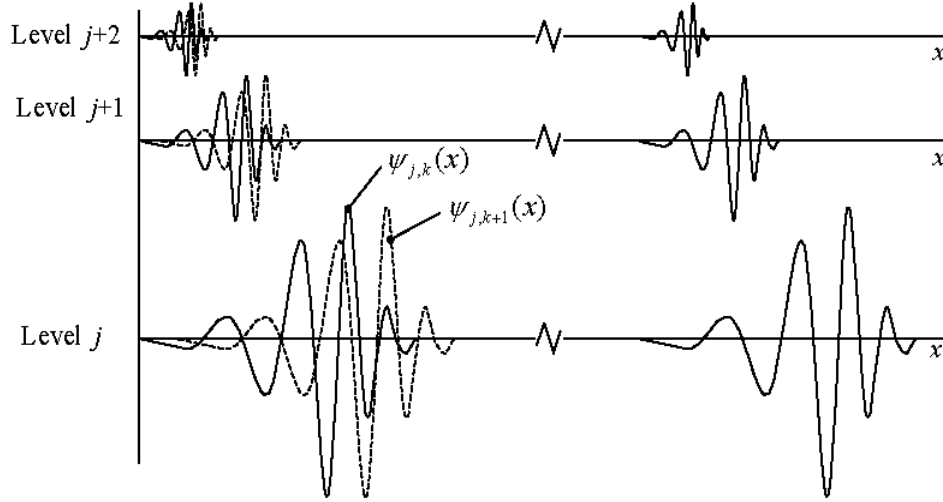


**Figure 1. D20 wavelet function at several different wavelet levels.**

Wavelet analysis is a form of multiresolution analysis (MRA). The basic ideas behind MRA can be understood through a comparison with the Fourier transform. Each sine or cosine function used in the Fourier transform corresponds to a discrete frequency and is defined over the entire signal duration. In contrast, the wavelet transform consists of wavelet functions of varying lengths and bandwidths. Each Fourier function has the same resolution: the entire time domain and a single frequency. But each level of the wavelet decomposition corresponds to a different resolution in the time and frequency domains, hence the term multiresolution analysis. Low-level wavelets are longer in the time domain and correspond to narrow, low frequency bands, whereas high-level wavelet functions are shorter and are associated with wider, high frequency bands. Thus, the wavelet functions with the finest resolution in the time domain have the coarsest resolution in the frequency domain and vice-versa. This is illustrated schematically in Figure 2. Note that there is some overlap between the frequency bands associated with adjacent wavelet levels, but the overlap is small compared to the bandwidth. The scaling function corresponds to the lowest frequency band.

The wavelet transform of a discrete function consisting of  $2^N$  points is

$$f(x) \approx \sum_{j=J}^{N-1} \sum_{k=0}^{2^j-1} d_{jk} \psi_{j,k}(x) + \sum_{k=0}^{2^J-1} c_{Jk} \varphi_{J,k}(x) \quad (3)$$

where  $d_{jk}$  and  $c_{Jk}$  are coefficients that are usually computed using a cascading filter bank (Mallat [16]).

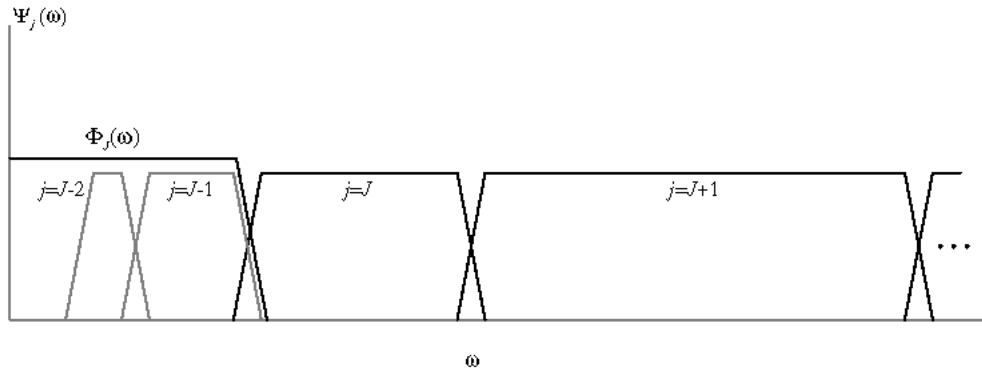


**Figure 2. Schematic representation of the frequency domain of different wavelet levels.**

### GROUND MOTION SIMULATION

Historical ground motions,  $a_g(t)$ , are typically available in a digitized format produced by sampling the analog accelerogram at evenly spaced time intervals. Therefore, the wavelet transform of  $a_g(t)$  can be expressed as

$$a_g(t) = \sum_{j=J}^{N-1} \sum_{k=0}^{2^j-1} d_{jk} \psi_{j,k}(t) + \sum_{k=0}^{2^J-1} c_{Jk} \phi_{J,k}(t) \quad (4)$$

which is the same as (3) with  $x$  replaced by  $t$ . In the following development, it is convenient to group the wavelet coefficients by level, so we rewrite (4) as

$$a_g(t) = a_\varphi(t) + \sum_{j=J}^{N-1} a_j(t) \quad (5)$$

where

$$a_\varphi(t) = \sum_{k=0}^{2^J-1} c_{Jk} \phi_{J,k}(t) \quad (6)$$

corresponds to the scaling function level and

$$a_j(t) = \sum_{k=0}^{2^j-1} d_{jk} \psi_{j,k}(t) \quad (7)$$

is the  $j$ th-level of the wavelet transform of  $a_g(t)$ . In Figure 3, we show an accelerogram from the 1994 Northridge earthquake recorded at the Rinaldi station plotted alongside its D20 wavelet decomposition. Note the significant localized temporal features in this record. Large amplitude wavelet coefficients in levels five and seven correspond to the prominent maxima in the input accelerogram. The sixth-level wavelets and the scaling function also exhibit noticeable nonstationary behavior. Above level eight, the amplitude decreases significantly with each successive wavelet level.

Several authors have observed a direct relationship between the wavelet coefficients and the evolutionary power spectrum of an accelerogram (Gurley [7], Basu [17]). This relationship follows directly from the compactness of the wavelet functions and the fact that at least one wavelet function in each level contributes to the signal at each point in time. The instantaneous power spectrum at time  $t$  can be expressed as the sum of the contributions from the wavelet functions that are nonzero at  $t$ . Because low-level wavelets have narrower frequency bands, this approximation is expected to have better resolution at low frequencies than at high frequencies. In Figure 3 we observed that the amplitude of the wavelet coefficients of a near-field accelerogram tended to be greater at low wavelet levels and decayed rapidly at the highest levels. Therefore, we will not introduce significant inaccuracies through coarser resolution in

the high frequency range or by approximating the narrow low frequency bands as discrete frequencies.

Under the assumption that each wavelet level in the decomposition (5) corresponds to a narrow band of frequencies that does not significantly overlap the frequency bands of adjacent wavelet levels, we propose that the stochastic process that caused a recorded accelerogram may be modeled as

$$\hat{a}_g(t) = Q_\phi a_\phi(t) + \sum_{j=J}^{N-1} Q_j a_j(t), \quad (8)$$

where  $Q_\phi$  and  $Q_j, j = J, J+1, \dots, N-1$  are uncorrelated time-invariant unit-mean Rayleigh random variables that represent the record-to-record variability in the amplitude, and hence energy, of the narrow band of frequencies associated with  $a_\phi(t)$  and  $a_j(t)$ , respectively. The theoretical justification for this model is discussed in reference [18]. Note that any temporal variations in the amplitude, phase and frequency content of the stochastic model (8) are completely defined by  $a_\phi(t)$  and  $a_j(t)$ . Furthermore, since

$$E[\hat{a}_g(t)] = E\left[Q_\phi a_\phi(t) + \sum_{j=J}^{N-1} Q_j a_j(t)\right] = E[Q_\phi] a_\phi(t) + \sum_{j=J}^{N-1} E[Q_j] a_j(t) = a_\phi(t) + \sum_{j=J}^{N-1} a_j(t) = a_g(t), \quad (9)$$

simulations based on (8) are unbiased in the time-domain.

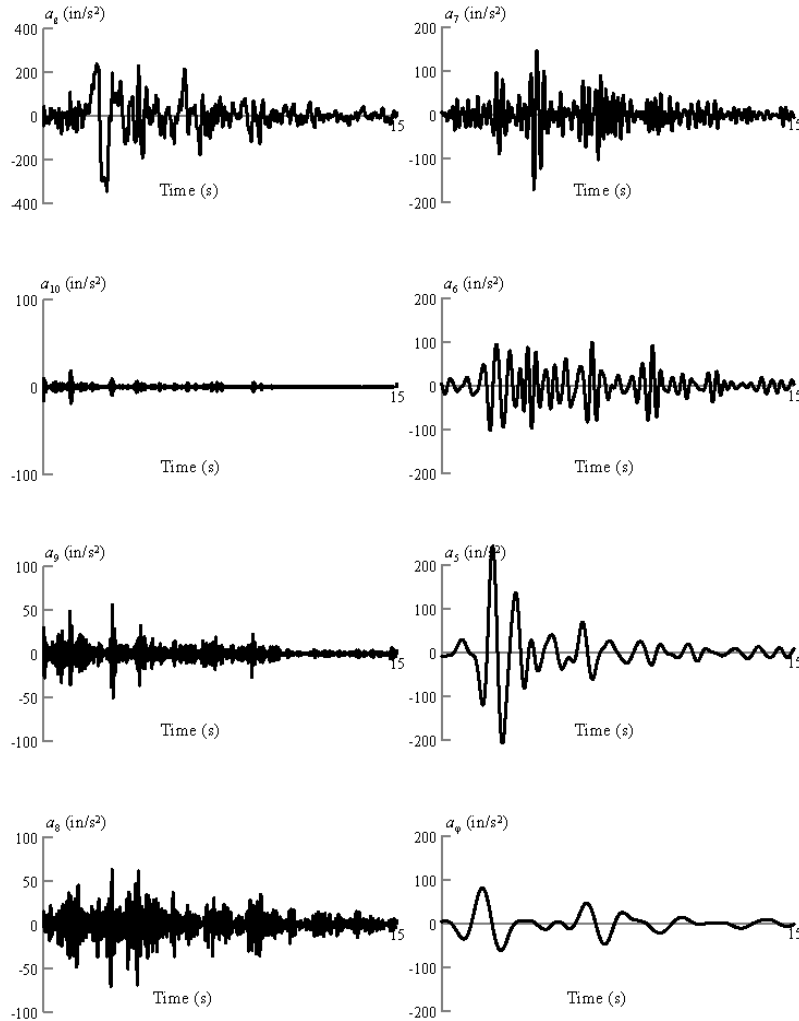


Figure 3. D20 decomposition of the Northridge earthquake recorded at Rinaldi receiving station.

Using the stochastic model (8) as a basis, the proposed wavelet-based simulation procedure used in this paper is implemented as follows.

1. Select a target accelerogram and pad the record with zeros until it has  $2^N$  values for some integer,  $N$ .
2. Select the lowest wavelet level  $0 \leq J \leq N$  to include in the wavelet decomposition (5). The value of  $J$  to be used can be based on the relative contribution of wavelet levels  $j < J$  to the total energy or significant temporal characteristics of the recorded accelerogram. In general however, one can select  $J = 0$  without any significant impact on the accuracy or efficiency of the procedure.
3. Generate  $N-J+1$  independent realizations of a unit-mean Rayleigh-distributed random variable,  $q_\phi, q_J, \dots, q_{N-J}$  and compute

$$\hat{a}_g(t) = q_\phi a_\phi(t) + \sum_{j=J}^{N-1} q_j a_j(t), \quad (10)$$

which is a simulated accelerogram that has significant temporal features similar to those present in the target record.

## ANALYSIS AND RESULTS

To examine the accuracy and utility of the proposed simulation procedure, we present the results of series of nonlinear time-history analyses performed with ensembles of wavelet-based and ARMA-generated synthetic ground motions. The recorded ground motions used as the bases for both the wavelet-based and ARMA simulations are listed in Table 1. These fault-normal near-fault ground motions were originally compiled for the second phase of the SAC Joint Steel Venture Project by Somerville [19]. The wavelet ensembles used in the analyses were generated with the D20 wavelet. The ARMA ensembles were generated with the moving-window procedure described by Conte [13].

**Table 1. SAC near-field ground motions.**

Earthquake	Year	$M_w$	Station	R (km)	ID
Northridge	1994	6.7	Rinaldi	7.1	N1
Tabas	1978	7.4	Tabas, Iran	1.2	N2
Loma Prieta	1989	6.9	Los Gatos	3.5	N3
Cape Mendocino	1992	6.5	Petrolia	8.5	N4
Northridge	1994	6.7	Olive View (Sylmar)	6.4	N5
Kobe	1995	6.9	JKMA	0.6	N6

Figure 4 shows three synthetic acceleration and velocity time histories produced from the Northridge Rinaldi ground motion (N1) using the above procedure. It is readily apparent that the prominent localized features of the input ground motion have been preserved in each synthetic time history. A corresponding set of three ARMA-generated simulations for N1 is shown in Figure 5. The strong initial pulse and several secondary pulses are present in the acceleration domain in each of the simulations. However, in the velocity domain, the amplitude of the pulse is well preserved, but its shape is severely distorted in all three simulations. A visual comparison of the ARMA and wavelet simulations suggests that both methods capture the localized features of the target ground motion in the acceleration domain, but it is evident that the wavelet method does a superior job of preserving duration and shape of the velocity pulse.

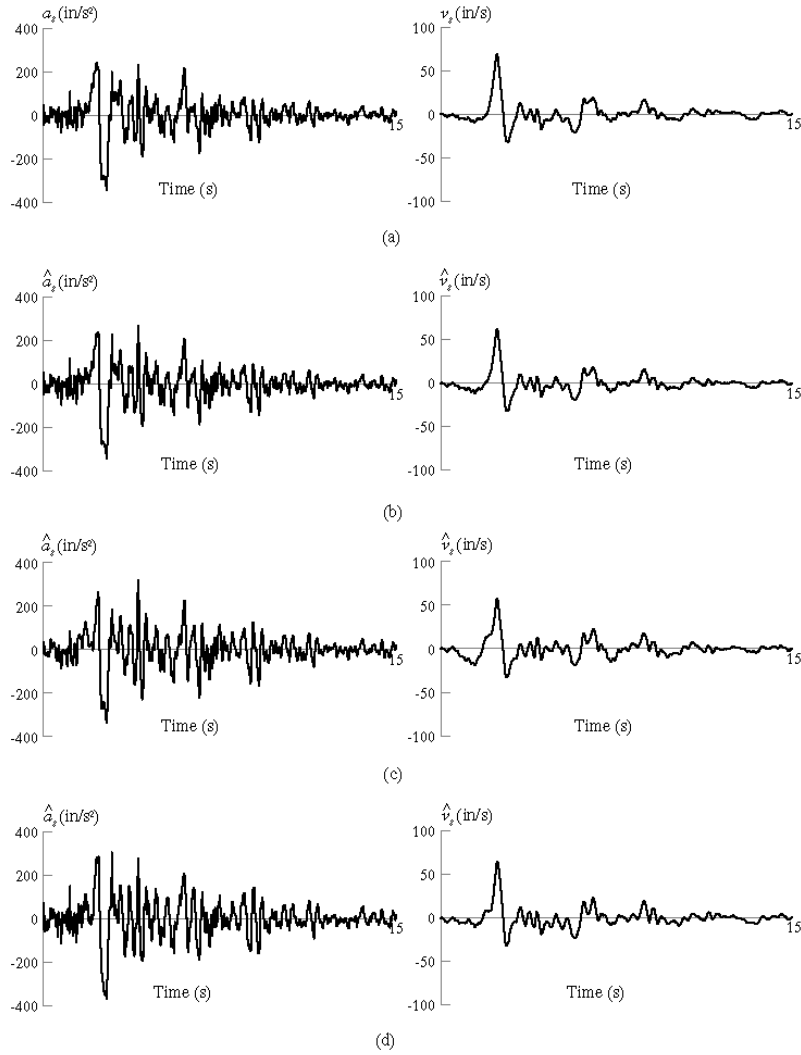


**Figure 4. N1 wavelet simulations: (a) target; (b-d) simulations.**

As an example of the quality of the artificial accelerograms obtained from these simulation procedures, consider the constant ductility response spectra for an ensemble of fifty synthetic ground motions based on record N1 shown in Figure 6. The figure shows the yield displacement required to achieve the specified ductility at each fundamental period. A strain-hardening ratio of 3% was used. Although some deviation is evident near the local extremes, the wavelet ensemble means closely match the target responses over the full range of periods. The ARMA ensemble means, on the other hand, exhibit the general trend of the targets, but fail to capture any of their localized characteristics.

To further examine the quality of the artificial ground motions generated by the proposed procedure, the nine-story building model shown in Figure 7 was analyzed using twelve ensembles of ten synthetic ground motions based on the records listed in Table 1 (six ensembles of wavelet-based simulations and six ensembles of ARMA-generated simulations corresponding to the six recorded ground motions). The moment-resisting frame of this building is proportioned in accordance with the building code requirements of Los Angeles and the provisions of FEMA 267 [20]. The design was originally commissioned for the SAC Joint Venture Steel Project. We investigated three aspects of structural response: maximum interstory drifts, interstory drift time histories, and maximum beam end rotation.

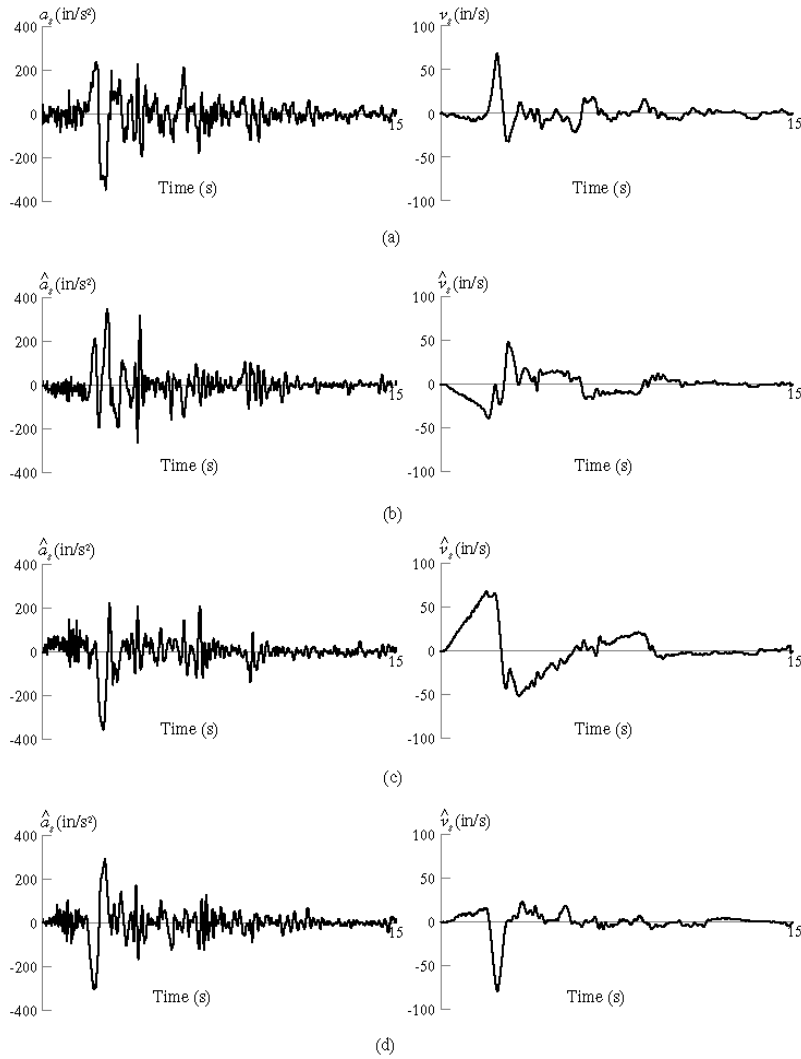


**Figure 5. N1 ARMA simulations: (a) target; (b-d) simulations.**

The maximum interstory drifts are plotted in Figures 8 and 9 for the wavelet and ARMA simulations, respectively. Note that the scale of the plots is different to accommodate the large drifts induced by the ARMA simulations. The ensemble means obtained for the wavelet-based simulations match the target drift profiles more closely than the ARMA ensemble means. For the N5 and N6 records, nearly all of the ARMA simulations produce higher drifts than the target. The wavelet ensembles, in contrast, are more evenly distributed above and below the targets. In general, there is also much more variation in the ARMA results than in the wavelet results. This variation appears to be independent of story height. For the most part, the drift profiles approximate the shape of the target drift profile for both procedures. Assuming a drift-proportional damage model, the ARMA simulations appear more likely to produce higher damage estimates than the target accelerograms. A bootstrapping analysis applied to these results showed that the COV of the ensemble mean was typically about 10% for the wavelet ensembles and on the order of 30% for the ARMA ensembles. This suggests that additional simulations are not likely to dramatically alter the wavelet results; however, the ARMA results may change somewhat if more simulations are performed.

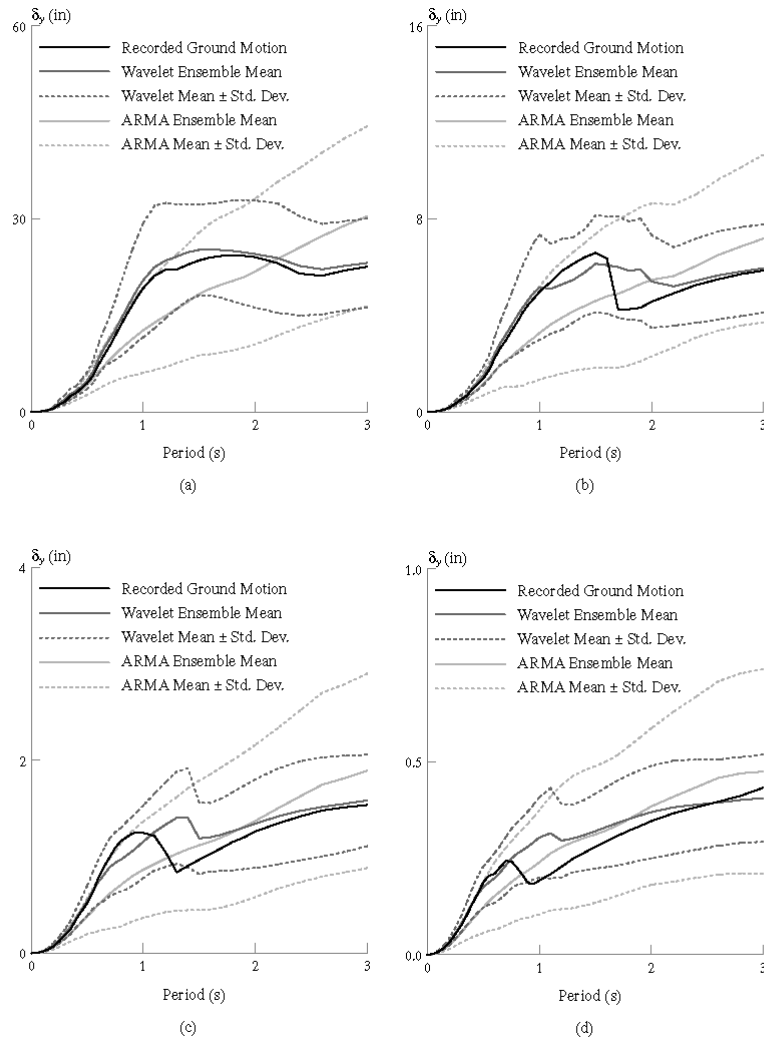


Figure 6. Constant ductility response spectra for N1: (a)  $\mu = 1$ ; (b)  $\mu = 2$ ; (c)  $\mu = 4$ ; (d)  $\mu = 8$ .

Level	Exterior column	Interior column	Girder	Seismic weight (kips)	Gravity load (psf)
9	W14X233	W14X257	W24X62	1010	90
8	W14X257	W14X283	W27X94	900	80
7	W14X257	W14X283	W27X102	900	80
6	W14X283	W14X370	W33X130	900	80
5	W14X283	W14X370	W33X141	900	80
4	W14X370	W14X455	W33X141	900	80
3	W14X370	W14X455	W33X141	900	80
2	W14X370	W14X500	W36X150	900	80
1	W14X370	W14X500	W36X150	900	80
0	W14X370	W14X500	W36X150	900	80

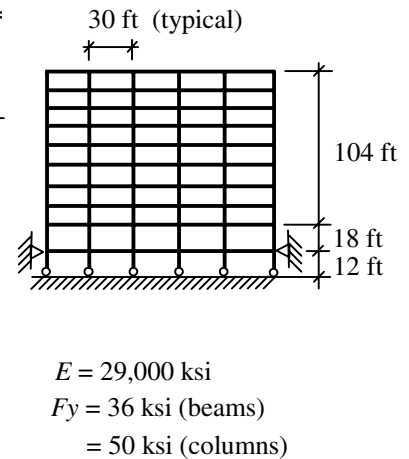
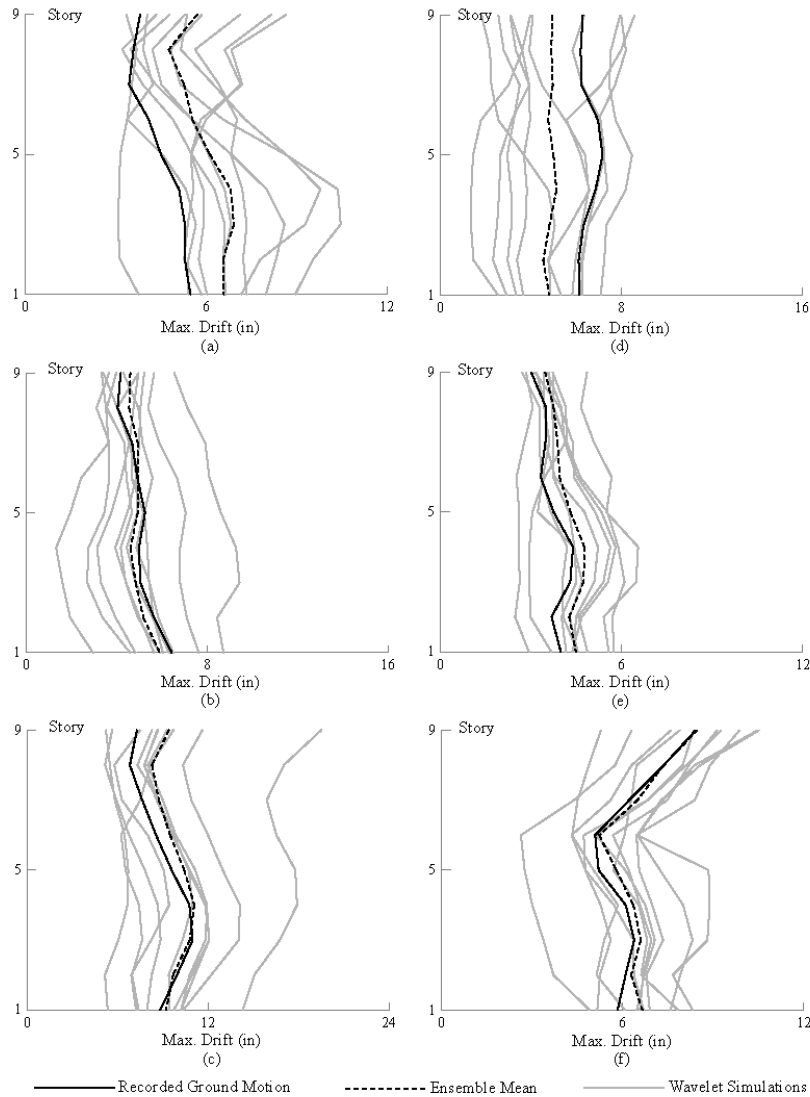


Figure 7. Example 9-story steel moment-resisting frame building.



**Figure 8. Maximum interstory drifts for wavelet ensembles.**

Figure 10 shows the story drift time histories for three wavelet and three ARMA simulations based on record N1 at the ninth story. Note that N1 imparts most of its energy in the first five seconds of the recording and the response after that point is essentially free vibration. The quantities of interest in these plots are the time and amplitude of the maximum story drift and, to a lesser extent, the number and amplitudes of the drift cycles. The wavelet simulations closely match the target: the peak drift occurs at roughly the same time as in the target and there are roughly the same number of cycles with similar amplitudes and durations to the target in each simulation. Furthermore, the initial pulse consisting of a negative peak followed by a broad positive plateau can be readily discerned in each of the wavelet simulations. Two of the ARMA simulations – Figures 10(g) and 10(h) – capture the first negative peak of the target, but neither of these simulations exhibits the positive plateau. Only one of the ARMA simulations – Figure 10(f) – has free vibration behavior similar to the target.

The maximum beam end rotations are compiled in Tables 2 through 7. The second column of each table lists the average rotation of the nine moment connections at each story for the target accelerogram. The third and fifth columns list the average rotations for the wavelet and ARMA ensembles taken over all nine

connections and all ten simulations. Coefficients of variation are also tabulated for each ensemble. To give some meaning to these values, experiments performed as part of the SAC project suggest that flange fracture of fully-restrained beam-column moment frame connections occurs at a rotation of roughly 0.04 radians and (based on a limited amount of experimental evidence) shear tab fracture occurs at a rotation of roughly 0.07 radians (see Figure 5-1 and Table 5-6 of FEMA 356 [21]). Note that the first floor beams are at ground level – the structure has a basement – and are laterally constrained, thus rotations at the first floor are much less than at other floors. Both sets of results tend to be greater than the targets, but the difference is much more pronounced for the ARMA ensembles. This is especially evident for N2, N5, and N6 where the ARMA mean rotations are 1.5 to 3 times the target values. The wavelet results, in contrast, are within  $\pm 50\%$  of the targets. The COV is typically between 30% and 60% for the wavelet ensembles, and between 50% and 80% for the ARMA ensembles. For the N1 ensembles the ARMA ensemble means are closer to the targets than the wavelet ensemble means, but the ARMA ensemble has twice the COV of the wavelet ensemble. Part of the reason for this may be seen in Figure 5.8(a). The maximum drifts of seven of the ten ARMA simulations lie below the target; however, two outlying simulations that produced very large drifts cause the mean to be biased.

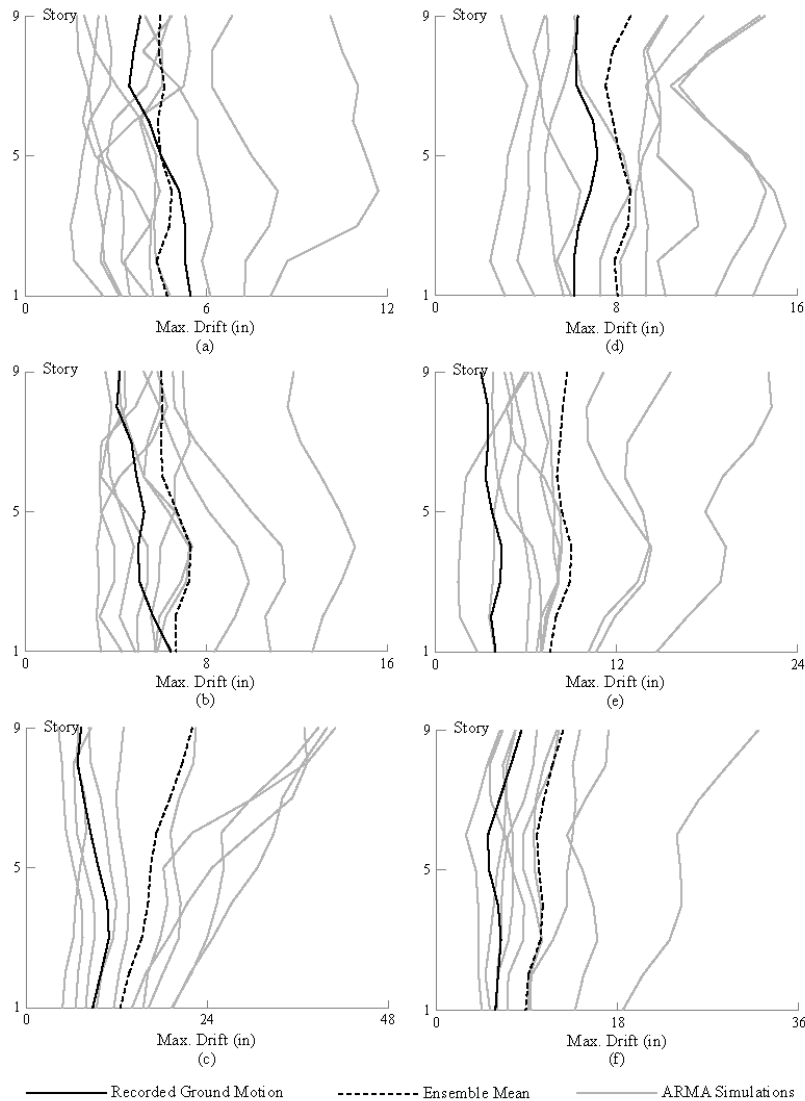


**Figure 9. Maximum interstory drifts for ARMA ensembles.**

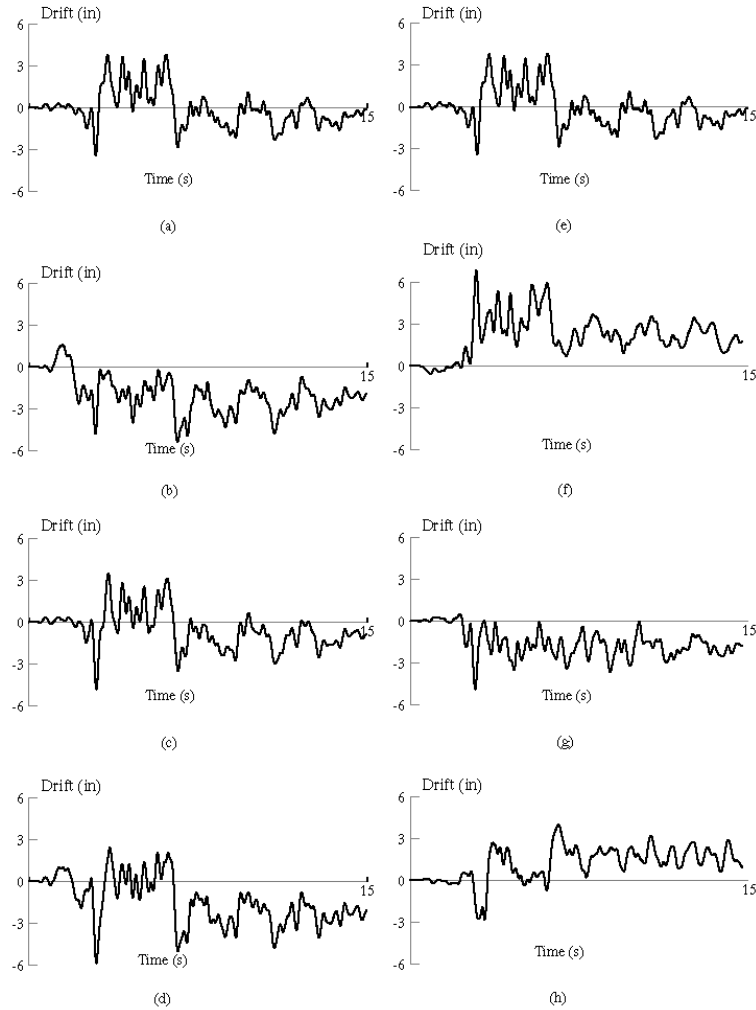


**Figure 10. Ninth story drift time history for N1 ensembles. (a,e) target; (b-d) wavelet simulations; (f-h) ARMA simulations.**

Based on the analysis results presented herein, it is apparent that the response of nonlinear systems to wavelet-based simulations tends to be nearer to the target response than the response to ARMA simulations. Additionally, the wavelet ensembles reproduced localized and time-varying response quantities that the ARMA ensembles failed to capture. Furthermore, the quality of the wavelet ensembles was more consistent, exhibiting less variation within simulated ensembles and between ensembles generated with different input accelerograms, than that of the ARMA ensembles. Whereas response to the wavelet simulations was typically well distributed above and below the targets, the ARMA simulations generally produced larger peak responses, both in terms of story drift and beam end rotation, than the targets. In some cases, the difference was more than 100%. This is an interesting result because one might expect the ARMA simulations to “miss” the near-field pulse and produce less intense simulations more consistent with far-field recordings. Instead, the ARMA simulations amplify and extend the pulse (see Figure 5), producing simulations that are more intense than the targets. As with all simulation methodologies, the quality of the simulations depends on the application. While we have highlighted the differences, there are some instances, such as the response of stiff structures, where the two methods produced similar results. Therefore, in some cases, the ARMA method may be adequate. However, the wavelet method consistently resulted in closer agreement with the target values over a wider range of systems and applications than the ARMA method.

**Table 2. Beam hinge rotations: N1.**

Lvl	Target	Wavelet		ARMA	
		Mean	COV	Mean	COV
1st	0.002	0.004	0.545	0.002	0.903
2nd	0.023	0.030	0.309	0.017	0.653
3rd	0.025	0.034	0.345	0.021	0.744
4th	0.025	0.036	0.366	0.023	0.782
5th	0.020	0.031	0.381	0.020	0.881
6th	0.018	0.027	0.324	0.018	0.921
7th	0.013	0.023	0.358	0.018	0.873
8th	0.015	0.021	0.365	0.020	0.778
9th	0.014	0.023	0.406	0.017	0.839
Roof	0.013	0.025	0.439	0.017	0.873

**Table 3. Beam hinge rotations: N2.**

Lvl	Target	Wavelet		ARMA	
		Mean	COV	Mean	COV
1st	0.004	0.003	0.650	0.004	1.056
2nd	0.027	0.024	0.409	0.030	0.600
3rd	0.025	0.023	0.509	0.035	0.568
4th	0.023	0.022	0.610	0.038	0.548
5th	0.023	0.020	0.582	0.035	0.580
6th	0.023	0.023	0.447	0.030	0.598
7th	0.020	0.021	0.388	0.026	0.655
8th	0.017	0.021	0.364	0.028	0.478
9th	0.016	0.017	0.408	0.027	0.469
Roof	0.016	0.018	0.355	0.026	0.554

**Table 4. Beam hinge rotations: N3.**

Lvl	Target	Wavelet		ARMA	
		Mean	COV	Mean	COV
1st	0.006	0.008	0.533	0.013	0.636
2nd	0.046	0.046	0.321	0.067	0.467
3rd	0.058	0.056	0.333	0.082	0.457
4th	0.061	0.061	0.318	0.090	0.458
5th	0.054	0.058	0.340	0.092	0.514
6th	0.047	0.052	0.362	0.094	0.580
7th	0.039	0.045	0.382	0.100	0.645
8th	0.036	0.043	0.409	0.114	0.686
9th	0.033	0.045	0.493	0.122	0.731
Roof	0.034	0.048	0.506	0.125	0.733

**Table 5. Beam hinge rotations: N4.**

Lvl	Target	Wavelet		ARMA	
		Mean	COV	Mean	COV
1st	0.003	0.002	0.598	0.007	0.781
2nd	0.027	0.019	0.552	0.037	0.557
3rd	0.031	0.021	0.544	0.043	0.570
4th	0.033	0.024	0.532	0.046	0.539
5th	0.035	0.023	0.604	0.043	0.537
6th	0.034	0.021	0.615	0.040	0.510
7th	0.032	0.020	0.600	0.037	0.462
8th	0.028	0.022	0.573	0.038	0.424
9th	0.029	0.020	0.682	0.041	0.555
Roof	0.029	0.020	0.743	0.043	0.588

**Table 6. Beam hinge rotations: N5.**

Lvl	Target	Wavelet		ARMA	
		Mean	COV	Mean	COV
1st	0.001	0.001	0.367	0.006	0.845
2nd	0.013	0.016	0.324	0.036	0.597
3rd	0.017	0.021	0.335	0.045	0.623
4th	0.020	0.023	0.351	0.049	0.646
5th	0.017	0.020	0.371	0.045	0.676
6th	0.013	0.017	0.367	0.041	0.701
7th	0.011	0.014	0.340	0.040	0.748
8th	0.014	0.015	0.227	0.043	0.764
9th	0.010	0.013	0.301	0.043	0.809
Roof	0.006	0.010	0.426	0.043	0.800

**Table 7. Beam hinge rotations: N6.**

Lvl	Target	Wavelet		ARMA	
		Mean	COV	Mean	COV
1st	0.003	0.004	0.485	0.008	0.901
2nd	0.025	0.028	0.222	0.043	0.600
3rd	0.032	0.033	0.269	0.052	0.606
4th	0.031	0.033	0.289	0.058	0.594
5th	0.027	0.029	0.337	0.055	0.636
6th	0.020	0.024	0.373	0.053	0.639
7th	0.024	0.026	0.299	0.052	0.662
8th	0.034	0.034	0.247	0.059	0.673
9th	0.039	0.039	0.240	0.064	0.685
Roof	0.042	0.042	0.269	0.067	0.671

## CONCLUSIONS

This paper describes a procedure that uses the wavelet transform to create ensembles of synthetic ground motions from existing ground motion recordings. Because wavelet functions are localized in the time and frequency domains, wavelet analysis is well suited to modeling and simulating nonstationary processes. The set of wavelet functions at each level is treated as a narrowband Gaussian process where the wavelet coefficients act as a modulating function and the wavelet function determines the frequency band of the process.

In order to preserve the temporal features of the input accelerogram, we uniformly scale each level of wavelet coefficients of the input by a unit-mean Rayleigh-distributed random variable. This results in simulations that have the same “shape” as the target. The proposed method does not require user-specified parameters aside from the target accelerogram and the wavelet function. The procedure is a three-step process. (1) Evaluate the wavelet transform of the target accelerogram. (2) Independently scale each level of the wavelet transform by a unit-mean Rayleigh random variable. (3) Calculate the inverse wavelet transform.

Ensembles of synthetic ground motions were created based on six fault-normal near-field accelerograms using the proposed method and, for comparison, an ARMA-based method. Several nonlinear analyses were performed with the wavelet- and ARMA-based simulations. Overall the wavelet ensembles matched the targets much more consistently than the ARMA ensembles. The ARMA simulations were on average more intense and resulted in greater estimates of displacement, drift, and damage than the wavelet simulations. In some cases, the ARMA simulations produced more than twice the target displacement. In contrast, the wavelet simulations rarely differed from the targets by more than 50% and were not biased with respect to the target values. Outliers were also less common in the wavelet ensembles than in the ARMA ensembles. The degree of variation in the ARMA results was significantly greater than for the wavelet results. In all, this suggests that the wavelet-based procedure produces simulations that are well-suited to nonlinear analysis and result in displacements that are similar to those produced by the target accelerograms.

## REFERENCES

1. Anderson JC, Bertero VV. “Uncertainties in establishing design earthquakes.” *Journal of Structural Engineering*, ASCE, 1987; 113:1709-1724.
2. Hall JF, Heaton TH, Halling MW, Wald DJ. “Near-source ground motion and its effects on flexible buildings.” *Earthquake Spectra*, 1995; 11:569-605.
3. MacRae GA, Morrow DV, and Roeder CW. “Near-fault ground motion effects on simple structures.” *Journal of Structural Engineering*, ASCE, 2001; 127:996-1004.
4. Bertero VV, Mahin SA, and Herrera RA. “Aseismic design implications of San Fernando earthquake records.” *Earthquake Eng. and Structural Dynamics*, 1978; 6:31-42.
5. Newland DE. “Wavelet analysis of vibration, Part 1: Theory.” *Journal of Vibration and Acoustics*, 1994; 116:409-416.
6. Newland DE. “Wavelet analysis of vibration, Part 2: Wavelet maps.” *Journal of Vibration and Acoustics*, 1994; 116:417-425.
7. Gurley K, Kareem A. “Applications of wavelet transforms in earthquake wind and ocean engineering.” *Engineering Structures*, 1999; 21:149-167.
8. Priestley MB. “Evolutionary spectra and non-stationary processes.” *Journal of the Royal Statistical Society Series B*, 1965; 27:204-237.
9. Iyama J, Kuwamura H. “Application of wavelets to analysis and simulation of earthquake motion.” *Earthquake Eng. and Structural Dynamics*, 1999; 28:255-272.

10. Shinozuka M, Deodatis G. "Stochastic process models for earthquake ground motion." *Probabilistic Engineering Mechanics*, 1988; 3:114-123.
11. Gasparini D, Vanmarcke EH. "Simulated ground motions compatible with prescribed response spectra." *Evaluation of Seismic Safety of Buildings Report No. 2*, Dept. of Civil Engineering, Massachusetts Institute of Technology, Cambridge, MA, 1976.
12. Kozin, F. "Autoregressive moving average models of earthquake records." *Probabilistic Engineering Mechanics*, 1988; 3:58-63.
13. Conte JP, Pister KS, Mahin SA. "Nonstationary ARMA modeling of seismic motions." *Soil Dynamics and Earthquake Engineering*, 1992; 11:411-426.
14. Thráinsson H, Kiremidjian AS. "Simulation of digital earthquake accelerograms using the inverse discrete Fourier transform." *Earthquake Eng. and Structural Dynamics*, 2002; 31:2023-2048.
15. Walnut DF. "An Introduction to Wavelet Analysis." Birkhäuser, Boston, MA, 2002.
16. Mallat S. "A theory for multiresolution signal decomposition: The wavelet representation." *IEEE Transactions on Pattern Analysis and Machine Intelligence*, 1989; 11:674-693.
17. Basu B, Gupta VK. "Non-stationary seismic response of MDOF systems by wavelet transform." *Earthquake Eng. and Structural Dynamics*, 1997; 26:1243-1258.
18. LeGrue JS. "A wavelet-based procedure for ground motion simulation". Engineering degree dissertation. Dept. of Civil and Environmental Eng., Stanford University, Stanford, CA, 2003.
19. Somerville P, Smith N, Punyamurthula S, Sun J. "Development of ground motion time histories for phase II of the FEMA/SAC steel project." Technical Report SAC/BD-97/04, SAC Joint Venture Steel Program, Sacramento, CA, 1997.
20. FEMA 267. "Interim Guidelines: Evaluation, Repair, Modification and Design of Welded Steel Moment Frame Structures." Federal Emergency Management Agency, Building Seismic Safety Council, Washington, DC, 1995.
21. FEMA 356. "Prestandard and Commentary for the Seismic Rehabilitation of Buildings." Federal Emergency Management Agency, Washington, DC, 2000.